Appl. Phys. A 68, 653–661 (1999) / DOI 10.1007/s003399900038

Applied Physics A
Materials
Science & Processing

Reversible and athermal photo-vitrification of $As_{50}Se_{50}$ thin films deposited onto silicon wafer and glass substrates

R. Prieto-Alcón[1], E. Márquez[1], J.M. González-Leal[1], R. Jiménez-Garay[1], A.V. Kolobov[2], M. Frumar[3]

[1] Departamento de Física de la Materia Condensada, Facultad de Ciencias, Universidad de Cádiz, Apdo 40, 11510 - Puerto Real (Cádiz), Spain
(Fax: +34-956/834-924, E-mail: emilio.marquez@uca.es)
[2] Joint Research Center for Atom Technology, National Institute for Advanced Interdisciplinary Research, 1-1-4 Higashi, Tsukuba-shi, Ibaraki 305, Japan
[3] Department of General and Inorganic Chemistry, Faculty of Chemical Technology, University of Pardubice, Legions Sq. 565, 53210 Pardubice, Czech Republic

Received: 3 August 1998/Accepted: 13 January 1999/Published online: 7 April 1999

Abstract. Photo-vitrification of $As_{50}Se_{50}$ thin films deposited onto silicon wafer and glass substrates has been studied using X-ray diffraction, far-infrared, and differential infrared spectroscopies. The optical study of this photo-amorphization effect has been carried out by two different methods enabling the determination of the average thickness and refractive index of a wedge-shaped thin film. The refractive-index behaviour of the as-evaporated, crystallized, and photo-vitrified $As_{50}Se_{50}$ films is analyzed within the single-oscillator approach. The optical-absorption edge is described using the non-direct transition model, and the optical energy gap is calculated. In the course of the vitrification of an $As_{50}Se_{50}$ thin film deposited on a silicon substrate the photo-oxidation of the film has been additionally detected and arsenic trioxide micro-crystals were formed on the surface of the film. Such oxidation has not been observed with $As_{50}Se_{50}$ films deposited on glass substrates, which demonstrates that the photo-vitrification phenomenon depends also on the type of substrate. Finally, it is concluded from the optical study that a reversible photo-darkening effect accompanies the photo-induced vitrification phenomenon.

PACS: 78.66.Jg; 78.70.Ck; 78.30.-j; 78.20.Ci

It has been observed that amorphous chalcogenides can undergo many light-induced structural changes [1]. These photo-structural changes, when reversible, are only observed in bulk glasses or well-annealed amorphous thin films, where they can be removed by annealing near the glass transition temperature, T_g [2, 3]. On the other hand, except for the metal photo-dissolution phenomenon, irreversible effects generally occur in metastable thin films. It has also been shown that illumination with high-intensity light can lead to photo-crystallization of amorphous $GeSe_2$ [4].

In the present paper, a systematic study of a novel photo-induced structural effect in amorphous chalcogenide materials, namely the athermal light-induced vitrification of $As_{50}Se_{50}$ thin films is reported. Such process has only been observed when an $As_{50}Se_{50}$ film is crystallized on a silica glass substrate [5, 6]. Going one step further, we present here an investigation of the photo-vitrification process of $As_{50}Se_{50}$ thin films deposited onto silicon wafer and silica glass substrates. This will allow us to demonstrate that the photo-vitrification is a substrate-dependent process. The use of silicon enables us to follow the changes of infrared transmission. The phenomenon is found to be reversible and we will expound the results obtained for the first two annealing–illumination cycles. This photo-structural change will be discussed, not only in terms of X-ray diffraction (XRD) measurements [5, 6], but also using far-infrared (FIR) spectroscopy, as well as differential infrared (DIR) spectroscopy. In addition, we have carried out the optical study of this phenomenon, using two different methods of determining the optical constants proposed both by Swanepoel [7, 8], which take into consideration the lack of thickness uniformity of the present thermally-evaporated chalcogenide glass films.

1 Experimental details

Bulk samples were prepared by direct synthesis from high-purity elements (5N), heated together in an evacuated quartz ampoule, at a temperature of $\approx 950\,^{\circ}C$, for about 24 h. After the synthesis the melt was air-quenched, resulting in a bulk glass of the required chemical composition. The glassy nature of the ingot was checked using X-ray diffraction (Philips, model PW 1710). Amorphous thin-film samples were prepared by thermal evaporation of the $As_{50}Se_{50}$ bulk glass onto silicon and glass substrates, in a vacuum of $\approx 10^{-6}$ Torr, in a coating system (Edwards, model E306A). During evaporation the deposition rate was $\approx 1\,nm\,s^{-1}$, this quantity having been continuously measured by a quartz-crystal monitor (Edwards, model FTM-5). Electron microprobe analysis of the as-deposited $As_{50}Se_{50}$ thin films indicated that the film stoichiometry is correct to $\pm$ 0.5 at. %. The samples were annealed at $\approx 150\,^{\circ}C$ ($T_g \approx 164\,^{\circ}C$) for periods of time of, typically, 72 h in a $\approx 10^{-3}$ Torr vacuum. The $As_{50}Se_{50}$ films were illuminated by use of a 500 W high-pressure mercury

lamp (Oriel, model 6285), through an IR-cut filter, providing broadband white light (significantly, with a very high UV output), using a light intensity of $\approx 50\,\mathrm{mW\,cm^{-2}}$. The typical light exposure time was about 10 h. X-ray diffraction, using Cu K_α radiation (1.54 Å), was used to examine the glassy or crystalline nature of the films. Mass measurements were made by a microbalance (Mettler, model AE200) to check possible changes as a consequence of the treatments.

The optical transmission spectra used in this study were obtained over the 300–2000 nm spectral region by a double-beam UV/Vis/NIR spectrophotometer (Perkin-Elmer, model Lambda-19). The spectrophotometer was set with a slit width of 1 nm. It was therefore unnecessary to make slit width corrections, since that value of the slit width was much smaller than the different linewidths. The area of illumination, over which a single optical transmission spectrum was obtained, was approximately $1\,\mathrm{mm} \times 10\,\mathrm{mm}$. The IR transmission spectra were measured by use of a FTIR spectrometer (Perkin-Elmer, model 2000) in the energy region 720–30 $\mathrm{cm^{-1}}$. A surface-profiling stylus (Sloan, model Dektak 3030) was used to determine the thickness of the films for the sake of comparison with the results derived from the optical transmission spectra: The thickness of the as-deposited films studied ranged mostly between around 700–1200 nm. The examination of the thin-film samples by scanning electron microscopy was carried out in a Jeol JSM-820 electron microscope. All measurements were made at room temperature and before them, films were kept in the dark.

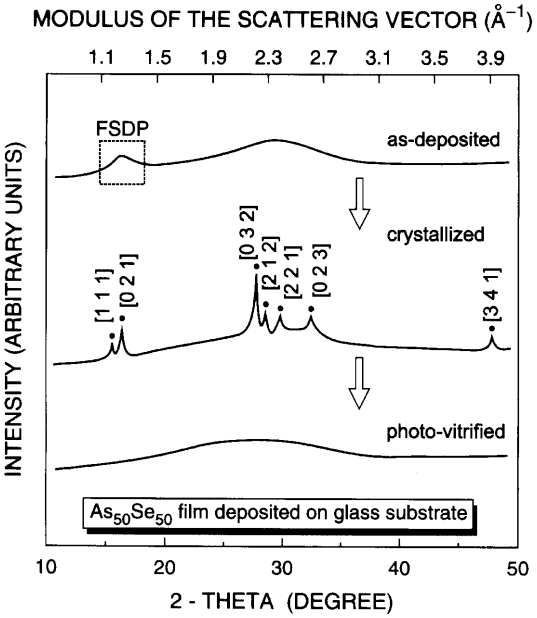

Fig. 1. XRD patterns (Cu K_α radiation) of the as-evaporated, crystallized, and photo-amorphized $As_{50}Se_{50}$ thin films, respectively, on a glass substrate

2 Results and discussion.

2.1 Structural analysis of the photo-vitrification process

2.1.1 X-ray diffraction study. X-ray diffraction patterns of as-evaporated, annealed, and illuminated $As_{50}Se_{50}$ films, deposited onto glass substrates, are shown in Fig. 1, and the corresponding XRD patterns of $As_{50}Se_{50}$ films, deposited onto silicon wafer substrates, can be seen in Fig. 2. Note the presence of the first sharp diffraction peak (FSDP) in the XRD pattern of the as-evaporated $As_{50}Se_{50}$ film deposited on a glass substrate, and virgin and illuminated $As_{50}Se_{50}$ films deposited on silicon wafers. This significant feature of the diffraction results on amorphous chalcogenides, has been ascribed to the influence of medium-range order [9, 10], and almost invariably occurs at a value of the modulus of the scattering vector of $\approx 1\,\mathrm{Å^{-1}}$ in these particular glassy materials.

Although most chalcogenide glasses are certainly quite reluctant to crystallization, $As_{50}Se_{50}$ thin films deposited on either glass or silicon substrates, could be crystallized by thermal annealing at $\approx 150\,^\circ\mathrm{C}$ for around 72 h, and comparison of the XRD patterns of the crystallized films with powder-diffraction data for As-Se crystals [11], revealed that the crystalline phase is c-As_4Se_4. It is important to note the virtual absence of the FSDP at $2\theta = 17^\circ$, characteristic of the amorphous phase, in the crystallized products. It is probable that a more prolonged thermal annealing period would lead to a further increase in the fraction of crystallized product, but this annealing was not attempted.

The fact that the relative peak intensities measured in our experiments are different from the reference powder-diffraction data, seems to suggest possible preferred orientational effects in the crystallized films. Such orientational effects, along with the extent of crystallization, have been shown to be dependent on the $As_{50}Se_{50}$ film thickness, when glass is the substrate used [12]. Thus, the crystallization of amorphous $As_{50}Se_{50}$ films, evaporated onto glass substrates, exhibits the following characteristics, as reported in [12]. In thin films (200–500 nm), the crystallization is very incomplete; in medium-thickness films (1000–2000 nm) there is only one strongly pronounced peak at 27.7°, which implies a preferred orientation of the crystallites with respect to the plane of the substrate. In contrast, thick films (3000–5000 nm) show an XRD pattern where numerous peaks are resolved, although the most intense peak appears again at $2\theta = 27.7^\circ$. Additionally, peaks at $2\theta = 15.1^\circ$, 16.0°, 28.4°, and 32.7° are exhibited in common by both medium-thickness and thick samples.

Our film thicknesses, in the range 700–1200 nm, correspond to the medium-thickness case of [12]. The XRD pattern of our $As_{50}Se_{50}$ crystallized films on glass substrates (Fig. 1), present the most intense peaks at $2\theta = 27.59^\circ$ and 16.20°. In addition, less intense peaks are found at $2\theta = 15.31^\circ$, 28.58°, 29.90°, 32.64°, and 48.05°. If we compare these data with those obtained for $As_{50}Se_{50}$ crystallized films on silicon substrates (Fig. 2), we observe that many more peaks are resolved in the latter case. Apart from the peaks already found in the former case (except the peak at $2\theta = 48.05^\circ$), peaks at $2\theta = 23.36^\circ$, 33.06°, 34.85°, 40.45°, 41.75°, and 46.60° are clearly present in the XRD pattern of annealed $As_{50}Se_{50}$ films, deposited onto silicon wafer substrates. Thus, we can certainly assume that the crystallization process, which takes place upon annealing of medium-thickness $As_{50}Se_{50}$ films, is somewhat different, depending on the type of substrate involved. Furthermore, the different crystallization behaviour observed with films on a substrate, on the one hand, and scraped films and powdered glass, on the other, clearly indicates that there is a very important role played by the film–

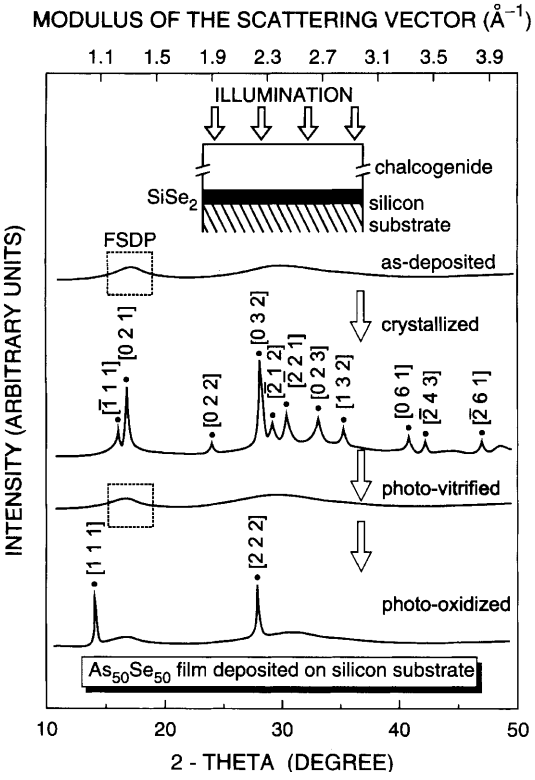

Fig. 2. XRD patterns (Cu K_α radiation) of the as-evaporated, crystallized, photo-vitrified, and photo-oxidized $As_{50}Se_{50}$ thin films, deposited onto silicon wafer substrates. The inset is a schematic representation of the annealed sample being illuminated, showing the possible formation of a thin layer of $SiSe_2$ on the interface of the amorphous chalcogenide with Si

substrate interface, and mechanical strain is very probably involved. In fact, crystallization might be enhanced by crystallization centres on Si wafers or by thin layers of formed $SiSe_2$ on the interface between the amorphous chalcogenide and silicon.

The crystallized $As_{50}Se_{50}$ films were subsequently exposed, in air, to white light from the mercury arc lamp for a period of time of about 10 h, at room temperature, which caused the complete disappearance of the crystalline features in the corresponding XRD pattern (see Figs. 1 and 2). This observation obviously implies the photo-amorphization of the present $As_{50}Se_{50}$ films, whether they are deposited onto glass or silicon wafer substrates. It is worthy of note that the temperature increase of the $As_{50}Se_{50}$ films during the irradiation process, as measured by a thermocouple conveniently affixed to the surface of the samples, was never more than $\approx 25\,^{\circ}$C. This observation gives unambiguous evidence of the athermal character of the photo-induced amorphous-state transformation. Interestingly, this temperature increase represents an advantage because, considering that the photo-vitrification phenomenon was found to be thermally activated [5], with $\Delta E_{\mathrm{ph}} = 0.15$ eV, the illumination time necessary to vitrify the film is reduced by around 35%.

Significantly, one differentiating structural characteristic of the photo-vitrification effect which takes place using a glass substrate, in relation to that which occurs when a silicon wafer substrate is used, is the total disappearance of FSDP in the former. In the latter, the FSDP does not disappear, although it becomes somewhat broader in the light-amorphized state. On the other hand, in [5, 6] a quartz–tungsten halogen lamp is used, and it is observed that both XRD patterns of as-evaporated and photo-vitrified $As_{50}Se_{50}$ films, deposited onto glass substrates, show basically the same features, including the FSDP. This fact may be due to the remarkable difference between the spectral irradiances of the two light sources employed, since the mercury lamp has a much higher UV light content than the quartz–tungsten halogen lamp, and so, part of the photons will have higher energy and will obviously produce a larger degree of disorder in the chalcogenide material. This observation suggests that the type of radiation is another factor to be taken into account, when an $As_{50}Se_{50}$ crystallized film is to be light-amorphized.

The crystallization–vitrification process was found to be reversible, with both types of substrates used in this work. That means that the photo-vitrified film, could again be crystallized by thermal annealing at $\approx 150\,^{\circ}$C, and then, vitrified once more by the corresponding illumination. We have performed three such cycles on a representative sample, with both types of substrates.

When the time of exposure of an $As_{50}Se_{50}$ crystallized film, deposited on a silicon wafer substrate, was approximately doubled (around 20 h), we found that apart from the photo-vitrification phenomenon, an additional photo-induced effect does seem to take place, the photo-oxidation of the sample. Consequently, new crystalline peaks arise upon irradiation of the annealed film (see Fig. 2), which could be explained in terms of a photo-oxidation of the $As_{50}Se_{50}$ film and the formation of arsenic trioxide. Thus, the XRD pattern of the overexposed $As_{50}Se_{50}$ film shows two peaks at $2\theta = 14.02^{\circ}$ and 28.04° (see ASTM card 36-1490). These findings are, at first sight, in agreement with the appearance of As−O chemical bonds, as indicated by well-resolved vibrational bands at around 620 cm^{-1} and 800 cm^{-1}, in the infrared transmission spectrum of the overexposed sample, and will be discussed further below. This behaviour has certainly not been observed before, during the athermal photo-vitrification process, when glass substrates were used and, apparently, is a characteristic of such a photo-induced phenomenon, when the layer is deposited, instead, onto silicon wafers. The presence of chemical instability in amorphous As_2Se_3 films has already been reported by Trubisky and Neyhart [13]. The decomposition of this chalcogenide glassy material was considered to proceed by an oxidation reaction at the surface of the film, such as:

$$As_2Se_3 + 3/2O_2 \rightarrow As_2O_3 + 3Se\,. \qquad (1)$$

In fact, the oxidation process represented above is highly favourable, if we consider the calculated heat of that particular chemical reaction, $\Delta H = -124$ kcal/mole. As_2O_3 micro-crystals were identified in this case and, thus, that reaction seemed to describe the source of chemical instability in a-As_2Se_3 films. However, the possible effect of light was not studied in those particular experiments. Comparison of a-As_2Se_3 films that were stored in complete darkness with some that were stored under daylight conditions, showed that As_2O_3 micro-crystals were much more numerous on those that had been exposed to visible white light. This observation clearly indicates that there is an important role played by

light in this oxidation process. A similar conclusion was made in [14].

Another mechanism has been proposed to explain the decomposition of *a*-As_2Se_3 films [12]. This mechanism considers a first step in which, as a consequence of the interaction with light, some elemental arsenic would be liberated. Subsequently, the liberated arsenic would be oxidized in the following manner:

$$4As + 3O_2 \rightarrow 2As_2O_3 \,. \tag{2}$$

On the other hand, we propose that the oxidation of As_2Se_3 films could also be envisaged by the following chemical reaction:

$$2As_2Se_3 + 9O_2 \rightarrow 2As_2O_3 + 6SeO_2 \,. \tag{3}$$

For As_4Se_4, we finally suggest the analogous oxidation reactions, which should be:

$$As_4Se_4 + 3O_2 \rightarrow 2As_2O_3 + 4Se \tag{4}$$

or

$$As_4Se_4 + 7O_2 \rightarrow 2As_2O_3 + 4SeO_2 \,. \tag{5}$$

The enhanced oxidation of $As_{50}Se_{50}$ on Si wafers can be connected with the fact that on the interface of the amorphous chalcogenide with Si, the following chemical reaction (possibly enhanced by illumination) can take place:

$$As_4Se_4 + 2Si \rightarrow 2SiSe_2 + 4As \,, \tag{6}$$

and created arsenic is then more easily oxidized, according to (2). Such a reaction can also proceed during annealing. Either $SiSe_2$ or Si can form crystallization centres which result in more pronounced X-ray patterns.

2.1.2 Far-infrared and differential infrared spectroscopies. Typical far-infrared transmission spectra for as-deposited, crystallized, and photo-amorphized $As_{50}Se_{50}$ films, onto silicon wafer substrates, are shown in Fig. 3. The as-deposited film shows a broad band in the spectral region 200–250 cm^{-1} and five more bands at 172, 138, 110, 90, and 57 cm^{-1}. The main infrared feature around 240 cm^{-1} corresponds to As−Se bond-stretching vibrations [15, 16]. The band at 110 cm^{-1} has been assigned to $AsSe_3$ and As_2Se_3 pyramidal molecules [17, 18], whereas the appearance of a band at 172 cm^{-1} can be explained in terms of the deformational As−Se−As vibrations [19]. Polymeric Se mode is observed at 138 cm^{-1} (bond-bending mode of the Se chain) and Se_8 rings at 90 cm^{-1} [20, 21]. Additionally, there is a very significant, strong absorption band at 57 cm^{-1}. Although in $As_{50}Se_{50}$ there are prevailing As_4Se_4 molecules, it is reasonable to suppose that during evaporation, the following reactions proceed:

$$2As_4Se_4 \rightarrow 2As_2Se_3 + As_4 + Se_2 \tag{7}$$

or

$$3As_4Se_4 \rightarrow 4As_2Se_3 + As_4 \,. \tag{8}$$

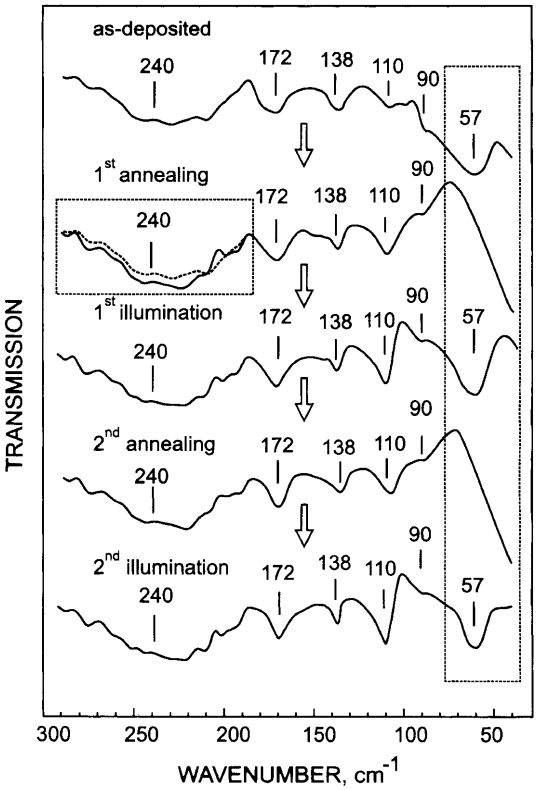

Fig. 3. Far-infrared spectra for the as-deposited, crystallized, and photo-amorphized $As_{50}Se_{50}$ samples, along with those for the crystallized and photo-vitrified $As_{50}Se_{50}$ samples, corresponding to a second cycle. There is a box showing how the main chalcogenide stretch peak has increased as a consequence of the first thermal annealing process

Se_2 can then be polymerized to Se_n chains. From those chemical reactions, it is clear that there should be excess of As or As plus Se, which would lead to the presence of As−As bond vibrations in the corresponding IR transmission spectra. The vibrations of As−As bonds in As−S system glasses can be found near 235 cm^{-1} and vibrations of As-rich structural units in the region of 130–260 cm^{-1} [22]. The fundamental broad band of AsS_3 pyramids vibrations can be found near 345 cm^{-1}. In As−Se system, due to Se, which is heavier than S, the fundamental vibrations of $AsSe_3$ pyramids are shifted towards lower frequencies, $\approx 240\ cm^{-1}$, as pointed out before, while the As−As vibration frequencies are probably unchanged. Due to large overlapping of both bands, the As−As bonds cannot be seen. There is another difficulty with the As−Se system spectra interpretation. The difference between atomic weights of As and Se is low and the vibrations frequencies of As−As, As−Se, and Se−Se bands in similar structural units are very close. The overlapping of their vibrations can be strong, especially in amorphous solids with broader IR bands, and, therefore, it is difficult to separate them and assign the vibrations to the individual modes.

The IR spectrum of the crystallized $As_{50}Se_{50}$ film shows the existence of bands at wavenumbers very close, indeed, to those already found in the spectrum of the as-deposited sample. Nevertheless, there is an outstanding difference between those IR transmission spectra: the complete disappearance of the vibrational band at 57 cm^{-1}, as a consequence of the thermal annealing process. In addition, the main chalcogenide stretch band seems to increase (see Fig. 3, in which

a box has been drawn to highlight this observation), indicating an increase in the As−Se bond density, as a result of the ordering of the film, induced by the corresponding thermal annealing. It is well known [23] that virgin As_2Se_3 glass films contain substantial density of homopolar bonds, which is notably reduced by annealing. Considering the short-range bond arrangement, it means that during annealing, the following reaction proceeds:

$$\text{As}-\text{As}+\text{Se}-\text{Se}\rightarrow 2\text{As}-\text{Se}\,. \tag{9}$$

A two-step mechanism has been proposed for that particular reaction [23]: (i) A first step, namely excitation, in which cleavage of homopolar As−As and Se−Se bonds is produced to yield the rather reactive, excited states, As* and Se*:

$$\text{As}-\text{As}\rightarrow 2\text{As}^{*}\ \text{and}\ \text{Se}-\text{Se}\rightarrow 2\text{Se}^{*}\,. \tag{10}$$

(ii) A second step, namely interaction, which proceeds by reaction of the above excited states, as represented below:

$$\text{As}^{*}+\text{Se}^{*}\rightarrow \text{As}-\text{Se}\,. \tag{11}$$

Illumination of the crystallized $As_{50}Se_{50}$ sample with a Hg arc lamp, gives rise to the presence again of the absorption band at 57 cm^{-1} in the IR spectrum of the corresponding exposed sample. The absorption bands assigned to As−Se bond vibrations, and those attributed to Se_n chains and Se_8 rings, which were observed in the spectra of both, the as-deposited and crystallized $As_{50}Se_{50}$ films, are also present in the photo-vitrified sample spectrum. Next, the $As_{50}Se_{50}$ film was subjected to a second annealing, followed by a second illumination treatment. The vibrational bands observed in the FIR spectra for the crystallized and photo-vitrified layers, corresponding to the second annealing–illumination cycle, are also displayed in Fig. 3. From the above results, we can conclude that there is a very clear change in the vibrational band at 57 cm^{-1}, whereas the other bands remain practically unchanged. This vibrational band could be connected with some intramolecular or lattice (blocks in amorphous solids) vibrations, although the first reason is more probable. The bending vibrations can not be excluded either.

As mentioned above, when the irradiation was prolonged up to ≈ 20 h, photo-oxidation of the $As_{50}Se_{50}$ layer occurred, as shown by X-ray diffraction analysis. This is further supported by the appearance of IR transmission bands, at around 620 cm^{-1} and 800 cm^{-1}, characteristics of As−O bonds in *a*-As_2Se_3 thin films. As also indicated before, this photo-oxidation effect during the course of the vitrification process has not been observed previously, and could be characteristic of the photo-vitrification phenomenon of $As_{50}Se_{50}$ films, when silicon is the substrate used. On the other hand, it has been shown recently that optical illumination of arsenic selenide glass layers produces arsenic trioxide [23]. However, rather long-time and intense illumination was needed, which seems to indicate that *a*-As_2Se_3 films are not so much sensitive to oxidation. During the illumination of thin-film arsenic chalcogenides, not only crystalline As_2O_3 can be formed, but also amorphous As_2O_3. The former can be obviously identified by X-ray diffraction and, also, by the presence of an intense IR absorption band at approximately 800 cm^{-1}, in the corresponding IR transmission spectrum; the latter presents an IR absorption band at around 620 cm^{-1}. In the experiment using an illumination time of ≈ 20 h, oxygen atoms can also be involved in the photo-induced changes, so that the excited state, As*, formed in a previous stage, as pointed out before, could undergo the following pathway:

$$\text{As}^{*}+1/2\text{O}_2\rightarrow \text{As}-\text{O}\,. \tag{12}$$

Differential infrared spectroscopy has also been performed, so that individual spectra were transformed into absorbance-frequency coordinates, then the spectra were subtracted, and the results were, finally, transformed back into transmission-frequency coordinates. In this way, the spectrum of the over-exposed film (OE) was compared to the spectrum of the annealed state of that film, and marked with the symbols, OE-A. The DIR spectrum OE-A displayed in Fig. 4, shows the increase of absorption at around 620 cm^{-1} and 800 cm^{-1} due to the photo-oxidation effect, and the simultaneous decrease of absorption around 240 cm^{-1}, indicating a clear decrease of the As−Se heteropolar chemical bonds, in the course of oxidation. At the same time, the vibrational band at 57 cm^{-1} is present, which, as seen previously, appears in the IR transmission spectra of the as-deposited and photo-vitrified thin-layer samples.

Finally, the crystalline structure of the annealed $As_{50}Se_{50}$ film is composed of As_4Se_4 molecules. These molecules have a cage-like structure, in which a square of Se atoms bisects a distorted tetrahedron of As atoms. The average As−As bond length in As_4Se_4 is 2.57 Å and the As−As−Se bond angle subtended at either one of the As atoms comprising the As−As bonds is 101.2°. If one compares those values with the corresponding bond distance and bond angle in *a*-As, 2.49 Å and 98°, respectively, it is found that they are larger in the case of the As_4Se_4 molecule. The intermolecular distances, less than 3.70 Å, are shorter than the predicted van der Waals distance of 4.0 Å, which could be associated with relatively strong intermolecular interactions. Since the present light-induced amorphization phenomenon is athermal, the ac-

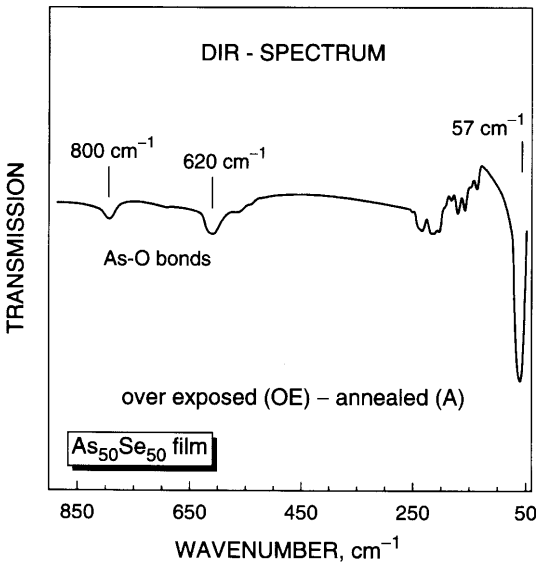

Fig. 4. Differential infrared spectrum of the overexposed film (OE) against the crystallized sample (A)

tion of the photons must certainly be to cause chemical bond breaking.

A possible mechanism to explain the phenomenon would involve intramolecular bond breaking of covalent bonds within the As_4Se_4 molecular units, to yield a cross-linked amorphous network. Nevertheless, there is another possibility, which would maintain the integrity of the As_4Se_4 molecules, although changes in their relative orientation and spatial distribution would occur, as a consequence of photo-induced intermolecular bond breaking. It has been suggested [24] that, since As−As distances and bond angles in As_4Se_4 are quite different from those in pure As, as clearly seen above, one can conclude that such intramolecular bonds are rather strained. As a result, the electronic states associated with these particular chemical bonds are likely to be at, or just above, the top of the valence band. Thus, optical illumination might be expected, preferentially, to involve the excitation of such electronic states, leading to bond cleavage; As−Se bond formation could then occur between closest atoms of neighbouring molecules, leading to a more cross-linked and disordered structure. In addition, intramolecular As−Se bonds may also be broken upon irradiation, giving rise to intermolecular As−Se bond formation.

Finally, a comparison of Raman spectra of crystallized and photo-vitrified layers shows that the spectrum of the former exhibits many narrow peaks characteristic of a molecular solid, whereas that of the latter exhibits instead just a single broad peak, characteristic of a cross-linked amorphous solid [24].

2.2 Optical study of the athermal photo-amorphization phenomenon

The optical study of the athermal photo-amorphization phenomenon has been carried out by two methods proposed both by Swanepoel, enabling the determination of the average thickness and refractive index of a wedge-shaped thin film. The first one is based on creating the upper and lower envelope curves of the optical transmission spectrum. In this particular method, it is assumed that the layer thickness, d, varies linearly over the illuminated area, so that the thickness is: $d = \overline{d} \pm \Delta d$ (see Fig. 5). Parameter Δd refers to the actual variation in thickness from the average thickness $\overline{d}$. The expressions for the top and bottom envelopes of the transmission spectrum, in the transparent region, are given as (11) and (12) from [7]. If the refractive index of the substrate alone is known, the above expressions are two transcendental equations with only two unknown parameters: the refractive index of the thin film, n, and the geometrical parameter, Δd. The validity range of this equation set is: $0 < \Delta d < \lambda/4n$, λ being the wavelength of incident radiation. All details about this first optical characterization procedure can be found in [7, 25, 26].

Figure 5 shows the optical transmission spectra corresponding to the as-evaporated, crystallized, and photo-vitrified $As_{50}Se_{50}$ films, for the first annealing–illumination cycle. The envelopes were carefully drawn using a computer program created by McClain et al. [27]. The average film thickness and thickness variation obtained by this particular optical characterization method from the spectra shown in Fig. 5, are given in Table 1. In all cases, the film thicknesses determined by mechanical measurements on the same film areas,

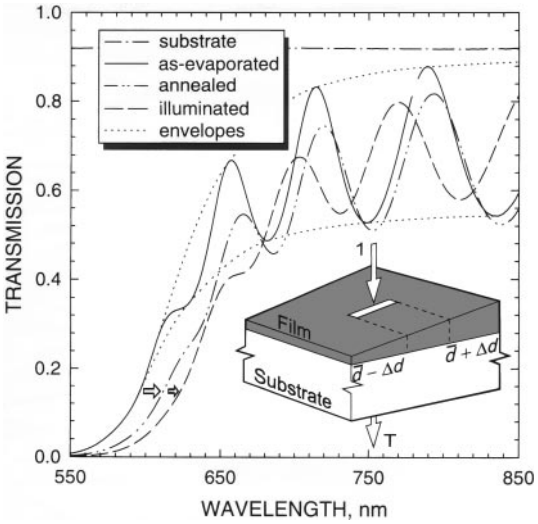

Fig. 5. Typical optical transmission spectra, in the short-wavelength region, for the as-deposited, crystallized, and photo-amorphized $As_{50}Se_{50}$ thin films, respectively. The upper and lower envelopes corresponding to the as-deposited film, are also presented as a representative example. In addition, a diagram showing a weakly absorbing thin layer with a linear variation in thickness on a thick transparent substrate

were in excellent agreement with the values calculated by the optical procedure – the difference being less than 2%. The obtained values of the geometrical parameter Δd show that it increases with the different treatments. The $As_{50}Se_{50}$ thin films submitted to a second annealing–illumination cycle show a higher degree of morphological alteration. Thus, taking into consideration that the applicability of this first optical characterization method is limited by the aforementioned condition, $0 < \Delta d < \lambda/4n$, an alternative procedure [8] was used. This second method is based on the transmission spectra at normal and oblique (30°) incidence, and allows determining the average thickness and refractive index of the samples corresponding to the second annealing–illumination cycle. A detailed explanation, and the results obtained by the application of this second optical characterization procedure to the thin-film samples that were subjected to a second annealing–illumination cycle, can be found in our previous work [28].

The decrease in the average thickness of the $As_{50}Se_{50}$ films due to annealing, $\approx 5\%$, is a sign of a thermal densification process (changes in the mass of the films were not observed), which leads to a structural compression as a consequence of the crystallization of the films. On the contrary, the increase found in the average thickness of the films, $\approx 4\%$, when they were exposed to bandgap light, could be a consequence of the photo-induced scission and weakening of intermolecular bonds, leading to an increase in the intermolecular separations, i.e., to an increase in free volume [29]. A subsequent thermal annealing of the thin-film sample would restore the chalcogen atoms bordering internal surfaces to their original positions, thereby decreasing again the volume of the sample. It is known that the free volume of amorphous solids is higher than that of crystalline solids.

From the values of the refractive index obtained, using either of both optical characterization methods, its spectral dependence is fitted to the Wemple–DiDomenico dispersion

relationship [30], that is, the single-oscillator model:

$$\varepsilon_1(\hbar\omega) = n^2(\hbar\omega) = 1 + \frac{E_0 E_\mathrm{d}}{E_0^2 - (\hbar\omega)^2} \,, \tag{13}$$

where $\hbar$ is Planck's constant divided by 2π, $\hbar\omega$ is the photon energy, E_0 is the single-oscillator energy (typically near the main peak of the $\varepsilon_2(\hbar\omega)$ spectrum) and E_d is the dispersion energy. By plotting $(n^2-1)^{-1}$ against $(\hbar\omega)^2$ and fitting a straight line as shown in Fig. 6, E_0 and E_d are determined directly from the slope, $(E_0 E_\mathrm{d})^{-1}$, and the intercept, E_0/E_d, on the vertical axis. The values of the dispersion parameters E_0 and E_d for the as-evaporated, crystallized, and photo-vitrified films are listed in Table 1 (two annealing–illumination cycles). The trend of E_0 is such that it is verified that $E_0 \approx 2 \times E_\mathrm{g}^\mathrm{opt}$, $E_\mathrm{g}^\mathrm{opt}$ being the optical band gap that will be introduced below (see Table 1) [31], whereas E_d according to Wemple and DiDomenico obeys the empirical relation [30, 32]:

$$E_\mathrm{d} = \beta N_\mathrm{c} Z_\mathrm{a} N_\mathrm{e}(\mathrm{eV}) \,, \tag{14}$$

where N_c is the coordination number of the cation nearest-neighbour to the anion, Z_a is the formal chemical valency of the anion, N_e is the effective number of valence electrons per anion and $\beta = 0.37 \pm 0.04$ eV for covalent crystalline and amorphous materials.

According to Wemple, the following relationship was proposed [32]:

$$E_\mathrm{d}^\mathrm{a}/E_\mathrm{d}^\mathrm{x} = \left(\rho^\mathrm{a}/\rho^\mathrm{x}\right)\left(N_\mathrm{c}^\mathrm{a}/N_\mathrm{c}^\mathrm{x}\right) \,, \tag{15}$$

where ρ is the mass density (we could instead use the film thickness), and 'a' and 'x' refer to the amorphous and crystalline forms, respectively. In order to explain the variation in the oscillator strength observed when an as-deposited $As_{50}Se_{50}$ film is annealed, or a crystallized film is illuminated, we have to take into account the thermal densification process in the first case, and the photo-induced volume expansion in the second. We will now point our discussion to the first annealing–illumination cycle (although this analysis is also qualitatively valid for the second annealing–illumination cycle). As a consequence of the annealing process, an increase of $\approx 7\%$ is observed in the E_d value. Then, if we make use of (15), we find that the difference between N_c, before and after annealing, is less than 2%; therefore, the small change in N_c indicates a rather insignificant change in the average coordination number in the short-range region. Additionally, E_d calculated from (14) (considering $N_\mathrm{c} = 3$, $Z_\mathrm{a} = 2$, and $N_\mathrm{e} = (50 \times 5 + 50 \times 6)/50 = 11$ [32]) was found to be 24.42 ± 2.6 eV; that is, allowing the corresponding scatter in β, E_d is certainly close to the experimental values of the virgin and annealed films. On the other hand, if we compare the E_d values corresponding to the annealed and illuminated samples, it is found that there is a very large decrease of $\approx 24\%$ in this particular case, and there is a parallel decrease of the mass density of $\approx 4\%$. The extra 20% reduction in the E_d value could, in principle, result from a decrease in the effective As coordination number.

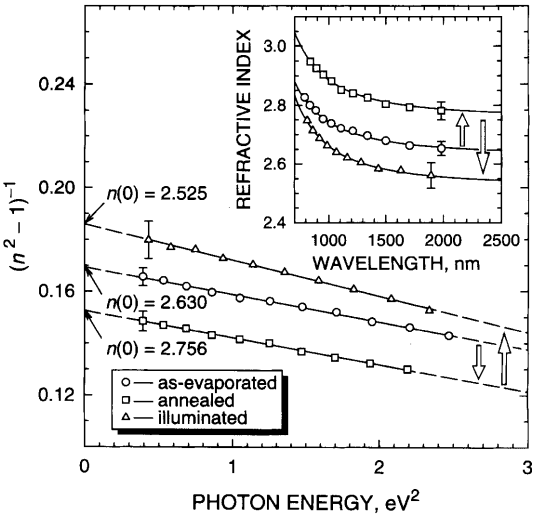

Fig. 6. Plot of the refractive-index factor $(n^2-1)^{-1}$ vs. $(\hbar\omega)^2$, for the as-deposited, crystallized, and photo-vitrified films, respectively; $n(0)$ values are the refractive indices extrapolated towards $\hbar\omega = 0$. The inset shows the refractive index vs. wavelength

Any of the aforementioned mechanisms proposed to explain the photo-vitrification process which, involve either intramolecular or intermolecular bond breaking, would obviously lead to a temporal decrease in coordination. However, this is also followed by the creation of new bonds after which the initial coordination may be restored. Thus, it seems reasonable to suggest that the effective coordination of the As atoms would not finally decrease, as a consequence of the bond breaking. Furthermore, if some homopolar As−As bonds are broken and new heteropolar As−Se bonds are formed, that could change the nature of the chemical bonding towards ionic, which would change the parameter β towards the smaller ionic value (in this particular case, $\beta = 0.26 \pm 0.03$ eV). Nevertheless, according to Paulings' electronegativities, the ionicity of As−Se bond is only $\approx 4\%$, so a small part of changed bonds from As−As to As−Se, can influence the ionicity of all bonds only a little. In addition, it should be pointed out that in ionic materials the more pronounced s–p splitting leads to s-like bands well below p-like bands, thus decreasing notably the parameter N_e [33].

Table 1. Values of the average thickness, $\overline{d}$, thickness variation, Δd, dispersion parameters, E_0 and E_d (single-oscillator analysis), optical band gap, $E_\mathrm{g}^\mathrm{opt}$, and Tauc slope, $B^{1/2}$ (Tauc's extrapolation), for the $As_{50}Se_{50}$ chalcogenide thin films under study

State	$\overline{d}$/ nm	Δd/ nm	E_0/ eV	E_d/ eV	$E_\mathrm{g}^\mathrm{opt}$/ eV	$B^{1/2}$/ $\mathrm{cm}^{-1/2}\,\mathrm{eV}^{-1/2}$
As-evaporated	1119 ± 10(0.9%)	18 ± 1	4.07 ± 0.02	24.08 ± 0.1	1.87 ± 0.01	785 ± 1
First annealing	1066 ± 11(1.1%)	28 ± 1	3.92 ± 0.03	25.86 ± 0.2	1.81 ± 0.01	770 ± 1
First illumination	1109 ± 19(1.7%)	34 ± 2	3.64 ± 0.03	19.56 ± 0.2	1.78 ± 0.01	770 ± 1
Second annealing	930 ± 35(3.8%)	–	3.83 ± 0.04	24.68 ± 0.2	1.81 ± 0.02	773 ± 2
Second illumination	1030 ± 39(3.8%)	–	3.68 ± 0.04	20.59 ± 0.3	1.73 ± 0.02	765 ± 4

On the other hand, continuing with the calculation of the optical constants, in the region of strong optical absorption, the procedure to obtain the absorption coefficient of non-uniform films is identical to the case of uniform films [7]. In this region the transmittance can be written in terms of the optical absorbance, x, by (22) from [34]. This optical parameter is related to the absorption coefficient, α, by the relationship: $x = \exp(-\alpha\overline{d})$. Since the optical absorbance and the average thickness are already known, the above relationship can be solved for α, thus yielding the absorption coefficient. The optical-absorption edges for the $As_{50}Se_{50}$ thin-film samples are displayed in the inset of Fig. 7. A clear shift to lower energies as a consequence of both annealing and illumination is clearly observed. In the high-absorption region ($\alpha > \approx 10^4\,\mathrm{cm}^{-1}$), assuming parabolic band edges and energy-independent matrix elements for interband transitions, the absorption coefficient is given according to Tauc [35] by the following equation:

$$\alpha(\hbar\omega) = B\frac{\left(\hbar\omega - E_{\mathrm{g}}^{\mathrm{opt}}\right)^2}{\hbar\omega}\,, \tag{16}$$

where B is an energy-independent constant, directly related to the width of the band tails, $\Delta E(\mathrm{tail})$. Formally, the optical gap is obtained as the intercept of the plot of $(\alpha\hbar\omega)^{1/2}$ against $\hbar\omega$. This graph is shown in Fig. 7 for the as-evaporated, annealed, and illuminated $As_{50}Se_{50}$ thin-film samples; the corresponding values of the Tauc gap, $E_{\mathrm{g}}^{\mathrm{opt}}$, and slope, $B^{1/2}$, are listed in Table 1. The values of the Tauc gap, thus determined, lead us to the conclusion that a clear reversible photo-darkening process accompanies the present photo-induced vitrification phenomenon. This conclusion is clearly supported by the above-mentioned FIR results. It is well known that As−As bonds play an important, although not predominant, role in reversible photo-darkening in well-annealed As-rich chalcogenide samples [3, 29]. An increase in the As−As bond concentration as a consequence of illumination, leads to a decrease of the Tauc gap, owing to formation of electronic states associated with such bonds, at the top of the valence band. Similarly, the subsequent annealing of the sample will lead to a decrease in the As−As bond concentration, and therefore, to an increase of the Tauc gap, because breaking of As−As bonds will replace electronic states in the gap associated with these homopolar bonds, by non-bonding As states located near the conduction band edge.

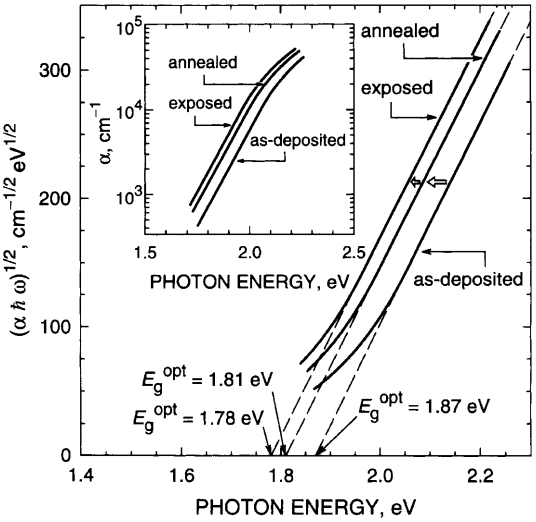

Fig. 7. Determination of the optical band gap in terms of the Tauc law, for the as-evaporated, annealed, and illuminated films, respectively, and in the inset the corresponding optical-absorption edges

3 Conclusions

The crystallization of amorphous $As_{50}Se_{50}$ thin films is shown to depend strongly on the type of substrate used. A different crystalline structure has been obtained for $As_{50}Se_{50}$ layers, evaporated onto glass and silicon wafer substrates, respectively. With the annealing temperature used in this work, $\approx 150\,^{\circ}\mathrm{C}$, the crystallization process has been found to be reversible, whether a glass or silicon substrate is involved. The crystalline products obtained at the above temperature exhibit the athermal photo-amorphization phenomenon. However, the photo-amorphization process of crystallized $As_{50}Se_{50}$ films deposited onto glass substrates, differs from that which takes place when those films are deposited onto silicon wafer substrates. The XRD patterns of the as-evaporated $As_{50}Se_{50}$ films, deposited onto glass substrates, and of the virgin and illuminated $As_{50}Se_{50}$ films, deposited onto silicon wafer substrates, show the significant presence of the FSDP at a value of the modulus of the scattering vector of $\approx 1\,\mathrm{\AA}^{-1}$.

Comparison of the reversible photo-vitrification phenomenon of crystallized $As_{50}Se_{50}$ layers deposited onto glass substrates, when those thin-film samples are exposed using two lamps with different spectral irradiances (mercury and quartz–tungsten halogen lamps), leads us to the conclusion that the radiation source is another relevant factor to take into account with regard to these experiments. Finally, an additional photo-induced change has been detected when silicon is the substrate used: The photo-oxidation of the $As_{50}Se_{50}$ chalcogenide film, with the corresponding formation of arsenic trioxide micro-crystals, and depends strongly on the time of exposure. No similar behaviour has been observed with glass substrates.

The morphological changes undergone by the wedge-shaped $As_{50}Se_{50}$ chalcogenide films, because of the successive thermal and optical treatments, made it necessary to use two different optical characterization methods for non-uniform thickness layers. One of them is based solely on the optical transmission spectrum at normal incidence, whereas the other is based only on the wavelengths of the tangent points of the upper and lower envelopes with the transmission spectrum, at normal and oblique (30°) incidence. The values of the optical constants and Tauc optical gaps derived by the aforementioned useful procedures, clearly evidence that a significant reversible photo-darkening process accompanies the present photo-induced amorphization phenomenon.

Acknowledgements. The authors would like to acknowledge some discussions with Dr. L. Tichý (Joint Laboratory of Solid-State Chemistry, Pardubice, Czech Republic). This work was supported by the CICYT (Spain), under the MAT98-0791 project.

References

1. J.S. Berkes, S.W. Ing, W. Hillegas: J. Appl. Phys. **42**, 4908 (1971)
2. Ke. Tanaka: Rev. Solid State Sci. **4**, 641 (1990)
3. G. Pfeiffer, M.A. Paesler, S.C. Agarwal: J. Non-Cryst. Solids **130**, 111 (1991)
4. J.E. Griffiths, G.P. Espinosa, J.P. Remeika, J.C. Phyllips: Phys. Rev. B **25**, 1272 (1982)
5. S.R. Elliott, A.V. Kolobov: J. Non-Cryst. Solids **128**, 216 (1991)
6. A.V. Kolobov, V.A. Bershtein, S.R. Elliott: J. Non-Cryst. Solids **150**, 116 (1992)
7. R. Swanepoel: J. Phys. E: Sci. Instrum. **17**, 896 (1984)
8. R. Swanepoel: J. Opt. Soc. Am. A **2**, 1339 (1985)
9. S.C. Moss, D.L. Price: In *Physics of Disordered Materials* (Plenum, New York 1985) p. 77
10. S.R. Elliott: Phys. Rev. Lett. **67**, 711 (1991)
11. Power Diffraction File, *Inorganic Phases*, JCPDS International Centre for Diffraction Data, 1988
12. A.V. Kolobov, S.R. Elliott: Philos. Mag. B **71**, 1 (1995)
13. M.P. Trubisky, J.H. Neyhart: Appl. Opt., Suppl. **3**, 59 (1969)
14. A.V. Kolobov, J.P. Badyal, R.M. Lambert: Surf. Sci. **222**, L819 (1989)
15. A.R. Hilton, C.E. Jones, R.D. Dobrott, H.N. Klein, A.M. Bryant, T.D. George: Phys. Chem. Glasses **7**, 116 (1966)
16. G. Lucovsky, R. Martin: J. Non-Cryst. Solids **8-10**, 185 (1972)
17. L. Zhenhua: J. Non-Cryst. Solids **127**, 298 (1991)
18. D.S. Ma, P.S. Danielsen, C.T. Moynihan: J. Non-Cryst. Solids **37**, 181 (1980)
19. Z.U. Borisova: In *Glassy Semiconductors* (Plenum, New York 1981) p. 59
20. T. Ohsaka: J. Non-Cryst. Solids **17**, 121 (1975)
21. T. Ohsaka: J. Non-Cryst. Solids **21**, 359 (1976)
22. M. Frumar, M. Vlcek, Z. Cernosek, Z. Polák, T. Wagner: J. Non-Cryst. Solids **213-214**, 215 (1997)
23. L. Tichý, H. Tychá, P. Nagels, E. Sleeckx: Opt. Mater. **4**, 771 (1995)
24. A.V. Kolobov, S.R. Elliott: J. Non-Cryst. Solids **189**, 297 (1995)
25. E. Márquez, J.B. Ramírez-Malo, P. Villares, R. Jiménez-Garay, R. Swanepoel: Thin Solid Films **254**, 83 (1995)
26. E. Márquez, J.M. González, R. Jiménez-Garay, S.R. Lukic, D.M. Petrovic: J. Phys. D: Appl. Phys. **30**, 690 (1997)
27. M. McClain, A. Feldman, D. Kahaner, X. Ying: J. Comput. Phys. **5**, 45 (1990)
28. C. Corrales, J.B. Ramírez-Malo, E. Márquez, R. Jiménez-Garay: Mater. Sci. Eng., B - Solid **47**, 119 (1997)
29. S.R. Elliott: J. Non-Cryst. Solids **81**, 71 (1986)
30. S.H. Wemple, W. DiDomenico: Phys. Rev. B **3**, 1338 (1971)
31. Ke. Tanaka: Thin Solid Films **66**, 271 (1980)
32. S.H. Wemple: Phys. Rev. B **7**, 3767 (1973)
33. T.I. Kosa, T. Wagner, P.J.S. Ewen, A.E. Owen: Philos. Mag. B **71**, 311 (1995)
34. R. Swanepoel: J. Phys. E: Sci. Instrum. **16**, 1214 (1983)
35. J. Tauc: J. Non-Cryst. Solids **8-10**, 569 (1972)